Super stretchable hexagonal boron nitride Kirigami

Tongwei Han[1*], Fabrizio Scarpa[2]*, Neil L. Allan[3]

[1]School of Civil Engineering and Mechanics, Jiangsu University, Jiangsu Zhenjiang 212013, P. R. China

[2]Advanced Composites Centre for Innovation and Science, University of Bristol, Bristol BS8 1TR, UK

[3]School of Chemistry, Cantock's Close, University of Bristol, Bristol BS8 1TS, UK

Abstract Kirigami, the ancient Japanese art of cutting and folding paper at the macroscale, has been recently applied to produce nanostructures with unusual deformation mechanisms. In this work we analyse the mechanical properties and deformation mechanisms leading to remarkable stretching and bilinear stiffness in armchair and zigzag hexagonal boron nitride (h-BN) Kirigami nanosheets using classical molecular dynamics simulations. We identify three geometric parameters that govern the mechanics and ductility of Kirigami h-BN. Enhancements in tensile strains up to 3-5 times higher than those of pristine h-BN can be obtained. The variations of stiffness, ultimate strength and strain with the parameters defining the Kirigami defect patterns can be used to tune the mechanical properties of h-BN and other nano 2D structures, potentially expanding their applications in bio-compatible strain-engineered nanodevices and nanoelectronics.

Keywords: hexagonal boron nitride; Kirigami; mechanical properties; molecular dynamics.

Corresponding author. E-mail address: f.scarpa@bristol.ac.uk, twhan@ujs.edu.cn

1. Introduction

Similar to graphene [1], hexagonal boron nitride (h-BN) [2-4] adopts a 2D nanostructure that has attracted significant interest in recent years due to its significant mechanical, electrical and chemical properties, and potential applications in nanotechnology [5-7]. The most distinctive advantages of BN nanomaterials over their carbon counterparts are that BN systems are electrically insulating [8, 9] and more stable at high temperature and in various chemical environments [10], combined with comparable levels of conductivity and mechanical performance [11-15]. Another important aspect of nano boron nitride systems is their bio-compatibility, which make them particularly suitable as active or passive nanoparticles for nanomedicine [16]. With this set of unique features, BN nanomaterials show great potential as components of nanoelectronic devices [17], functional nanocomposites [18, 19], hydrogen accumulators and other NEMS systems [20, 21]. Considerable efforts have been made to explore the mechanical properties of h-BN both from a theoretical and experimental point of view [15, 22, 23]. Similar to graphene, h-BN exhibits very high strength and stiffness values, with a Young's modulus ranging from 0.79 TPa to 0.97 TPa, and tensile strength between 120 GPa and 165 GPa [15]. However, the fracture strain of h-BN has been reported to lie between 0.13 and 0.27 (i.e., no more than 30%), which still limits the application of hexagonal boron nitride in strain-engineered nanodevices [24]. Developing approaches to enhance the ductility of 2D nanomaterials thus remains an open topic. The concept of Kirigami, an ancient Japanese art of cutting and folding paper, has been recently used to create complex 3D

multiscale structures [25-27], but also to pattern graphene experimentally into a variety of shapes including stretchable electrodes, springs, and robust hinges, which exhibit outstanding and tunable mechanical properties [28]. The Kirigami concept has also been applied to graphene and MoS_2 films, and molecular dynamics simulations have investigated the effectiveness of the Kirigami approach to improve the ductility and decrease the brittleness of 2D nanomaterials [29, 30].

This paper shows how to obtain a remarkable stretching and mechanical bilinear behaviour in hexagonal boron nitride sheets by applying cut patterns. So far, the mechanical behavior of h-BN nano-Kirigami systems has not yet been studied. The mechanical properties and deformation mechanisms of both armchair and zigzag [6] h-BN Kirigami systems are systematically investigated using classical molecular dynamics simulations. The influence of three geometric parameters related to pattern size on the tensile stress and strain and deformation mechanism is also investigated. These results provide guidelines for tailoring and manipulating the mechanical properties of h-BN or other nano 2D structures.

2. Molecular dynamics (MD) simulations

Our MD simulations used the LAMMPS (Large-Scale Atomic/Molecular Massively Parallel Simulator) open-source package [31], developed by Sandia National Laboratories. The Tersoff potential [32-34] was adopted for the interactions between the boron and nitrogen atoms, due to its success in previous studies of BN nanotubes and nanosheets [35-38]. Several sets of Tersoff or Tersoff-like potential parameters

have recently been developed for interactions between boron and nitrogen [39-46]. Sekkal et al. [39] and Verma et al. [40] obtained parameters to describe cubic BN and boron nitride nanotubes (BNNTs) respectively by small modifications of those for carbon. The boron nitride was treated as a one-component system. Matsunaga et al. [41, 46] considered c-BN as a two-component system with B-N interactions and proposed separate sets of parameters for boron and nitrogen atoms, which reproduce the lattice constants, bulk modulus and binding energy of cubic boron nitride. Albe et al. [42, 43] developed a Tersoff-like potential for BN, which is able to describe the sp^2 structures of BN polymorphs, BN clusters and pure B and N bonding. These potential parameters have been successfully employed in investigations of the structural, thermal and mechanical properties of BNNTs, h-BN nanosheets (BNNSs) and BN nanobamboos [35, 36, 47-49]. Recently, based on force-matching, adjusted Tersoff-like potential parameters [44, 45], obtained by fitting the obtained bond length and cohesive energy to experimental data, have also been used to simulate the thermal and mechanical behaviour of BN nanofillers and BNNSs [38, 44, 45, 50]. It is worth noting that the effective use of the Tersoff potential in the fracture analysis of 2D h-BN sheets remains a subject of debate. Modified Tersoff potential with the parameters B, R and D have been used to simulate the nanoindentation of cubic boron nitride[51]. However, other authors still use the original Tersoff potential of Kinaci et al. to account for the presence of Stone-Wales and other types of defects[52]. In the present MD simulations, the Tersoff-like potential with the parameters defined and proposed by Albe et al. [42, 43] was chosen, as shown in Table 1, due to its success in

predicting the stiffness and yielding effects of various BN nanostructures studied previously.

Tab.1. Tersoff-like interatomic potential parameters for BN [42, 43]

	BN-interaction	NN-interaction	BB-interaction
m	3	3	3
γ	1	1	1
λ_3 (Å^{-1})	1.9925	0	0
c	1092.9287	17.7959	0.52629
d	12.38	5.9484	0.001587
h	-0.5413	0	0.5
n	0.364153367	0.6184432	3.9929061
β	0.000011134	0.019251	0.0000016
λ_2 (Å^{-1})	2.784247207	2.627272104	2.077498242
B (eV)	3613.431337	2563.560342	1173.196962
R (Å)	2	2	2
D (Å)	0.1	0.1	0.1
λ_1 (Å^{-1})	2.998355817	2.829309329	2.237257857
A (eV)	4460.833973	2978.95279	1404.475204

The h-BN kirigami was constructed by making cuts in a h-BN nanoribbon with free edges. All cuts removed a whole number of BN formula units. The topology of the cuts is similar to those in single layer graphene sheets in Ref. [30]. A schematic view of the h-BN Kirigami showing the geometric parameters we vary is shown in Fig. 1. The key variables are the nanoribbon length L_0, the width b, the height and width of each interior cut (w and c) and the distance between successive cuts d. The edge cut length is defined to be half of the interior cut (ie. $0.5w$). For simplicity all interior and edge cut lengths are equal. The geometry parameters have been used to define nondimensional quantities for a subsequent parametric analysis of the mechanical performance of different configurations of the h-BN Kirigami sheets. We define the

ratio of the overlapping cut and sheet widths as $\alpha = (w\text{-}0.5b)/b$, the overlapping cut to sheet lengths $\beta = (0.5d\text{-}c)/L_0$[30], and the overall ratio between width and length of the h-BN sheet ($\gamma = L_0/b$). The cut width ratio α varies between -0.5 to 0.5 and controls the porosity of the Kirigami sheets, while the cut length ratio β (always a positive quantity) gives a measure of the density of the cuts, including the amount and width of the Kirigami geometric unit. In other words, the parameter α describes the geometry perpendicular to the loading direction, while the parameter β relates to the geometry parallel to the loading direction. The third parameter γ provides an indication of the scale effect when at constant α and β ratios. We consider both armchair and zigzag edges configurations for the sheets. The representative armchair h-BN Kirigami studied in this work has 9596 atoms, with a length $L_0 \sim 355.7$ Å, width $b \sim 100.2$ Å, height and width of each interior cut $w \sim 75.1$ Å and $c \sim 8.7$ Å respectively, and a distance between successive cuts $d \sim 43.4$ Å。

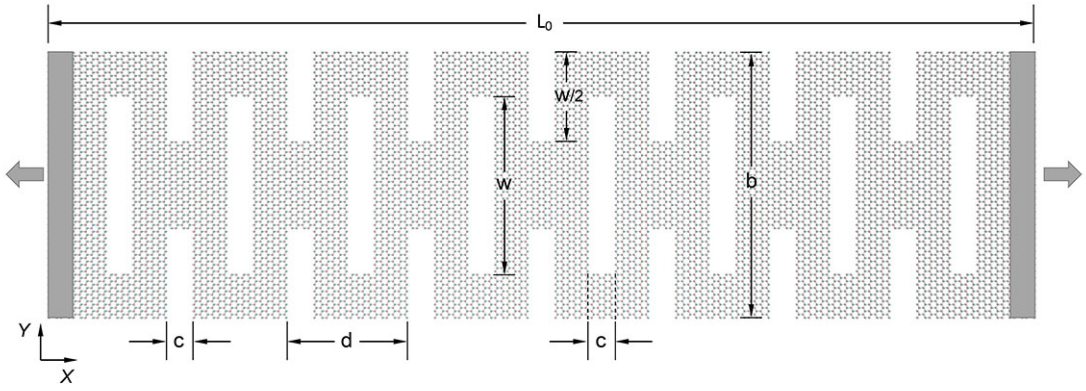

Fig.1 Schematic simulation model of the h-BN Kirigami, with the key geometric parameters labelled.

The h-BN Kirigami was first fully relaxed for at least 10000 time steps (each time step equal to 1fs) within a canonical (NVT) ensemble at 300 K. Subsequently, a

uniform displacement loading on the two opposite ends of the sheet was applied to stretch the Kirigami structure within the same NVT ensemble, until failure occurred. Nonperiodic boundary conditions were applied along all three directions, so that atoms do not interact across the boundary and do not move from one side of the box to the other. The equations of motion were solved using the velocity-Verlet algorithm [53] with a timestep of 1 fs. In individual simulations, the temperature was maintained at the specified value by using the Nose-Hoover method [54, 55]. The strain rate was set to 1×10^{9} s^{-1}. To obtain the stress-strain curves the virial stress in the loading direction was calculated for each strain [56]. The slope of the linear part of the curves gives the Young's modulus, and the ultimate strength and strain were taken as the maximum stress and strain before the onset of failure. Note that the equivalent Young's modulus of a pristine 2D h-BN system (within Kirigami) scales with its effective thickness, which in this work is 0.333 nm [40].

3. Results and discussion

3.1 Validation

To validate our MD simulations, we have simulated pristine h-BN nanosheets without Kirigami and calculated the Young's modulus, ultimate strength and strain. The stress-strain curves for armchair and zigzag h-BN nanosheets are shown in the inset of Fig. 2. First the Young's modulus obtained for armchair and zigzag h-BN are 874 GPa and 887 GPa, respectively, which compare with reported literature values of 790 GPa – 970 GPa from experiment [57], density functional theory [58, 59], MD [23, 60,

61] and structural mechanics methods [62, 63]. The values are also very close to those of boron nitride nanotubes [63-66]. The ultimate strength predicted by our models is 132 GPa for the armchair and 128 GPa for zigzag h-BN configurations. For comparison, values of 127 GPa and 114 GPa were calculated by Zhao et al. [61] previously in MD simulations using Tersoff potentials with parameters taken from Mastunaga et al. [41, 46] Moreover, the fracture strains obtained from our MD simulations at 300 K are 0.24 (armchair) and 0.36 (zigzag) (average 0.30) which are very close to corresponding values of 0.29, 0.32 and 0.305 (average) [60] and 0.28 (average) [61] strains calculated in previous MD simulations. The predictions contained in Ref [60] also clearly show the difference between the armchair and zigzag h-BN configurations, with the zigzag boron nitride sheet exhibiting ~ 10% higher strain to failure than the armchair one for a ~ 2:1 aspect ratio sheet. We observe also in our case a higher strain to failure for the zigzag configuration (~ 33%), which is justified by the higher slenderness ratio of the nanoribbons used in this work (3.55:1). We can therefore conclude that our present MD simulations are reliable in predicting the calculation of the tensile properties of h-BN nanosheets. The values of the ultimate strength and strain for the two pristine configurations (σ_U and ε_U) are used later to normalize the parametric curves describing the variation of the properties of the h-BN Kirigami sheets with different geometry parameters.

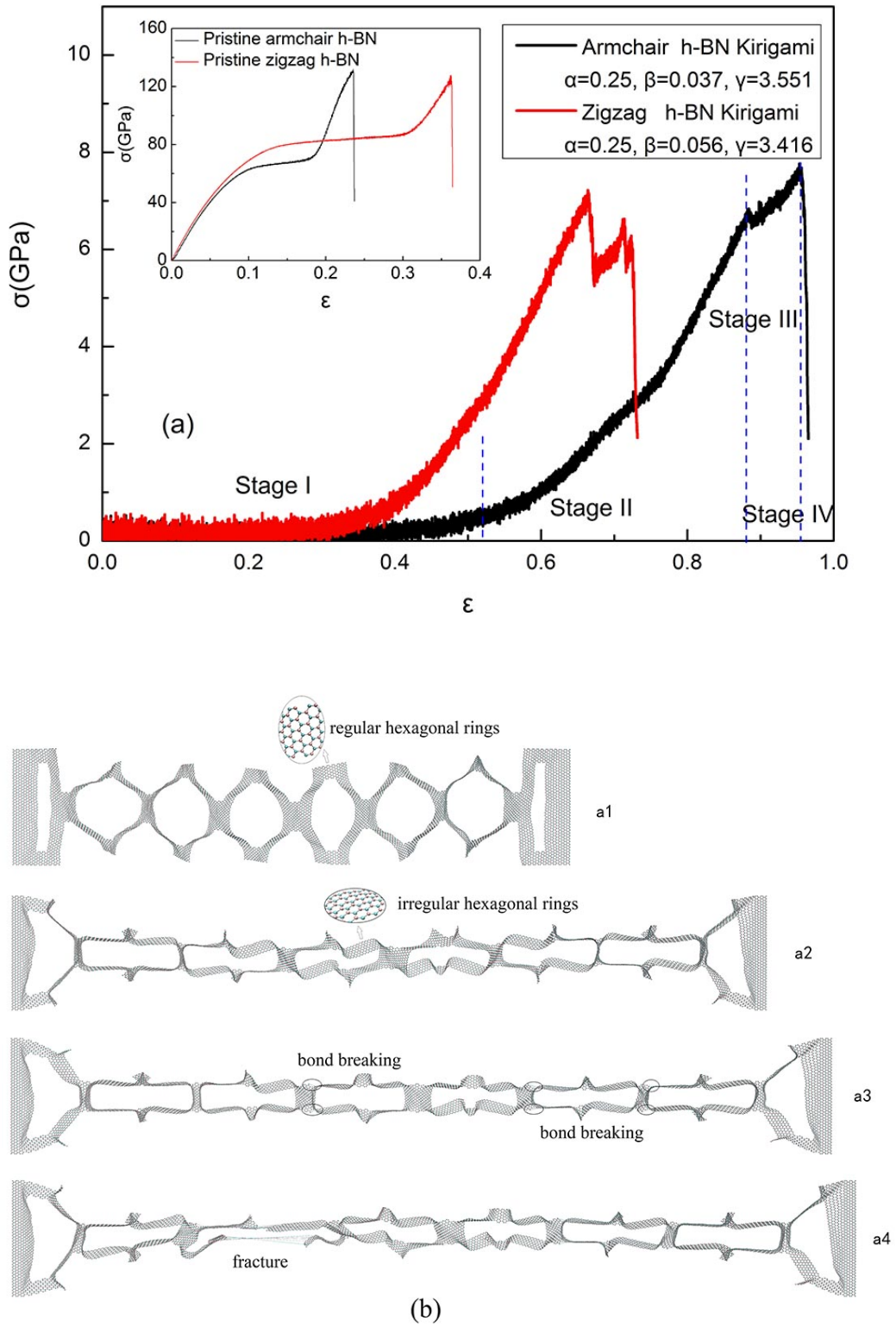

Fig.2 (a) Stress-strain curves of the representative armchair and zigzag h-BN Kirigami. Four distinct stages of deformation occur in the Kirigami sheets prior to failure, as shown in Fig. 2(a) by the dashed lines for armchair Kirigami. Stress-strain curves of

pristine armchair and zigzag h-BN are also shown in the inset for comparison. (b) Snapshots of the top view of the atom configuration of the armchair h-BN Kirigami. The tensile strains corresponding to the different stages are 30%, 78%, 91%, 96.3%, respectively. The snapshots were generated using Visual Molecular Dynamics (VMD) [67].

3.2 Stress-strain response and deformation mechanism of h-BN kirigami

Fig. 2 shows the stress-strain curves of the representative armchair and zigzag h-BN Kirigami and atom configurations at different deformation stages. Stress-strain curves of pristine armchair and zigzag h-BN are also shown in the inset of Fig. 2(a) for comparison. In contrast to pristine h-BN, the nanosheets with Kirigami cuts show markedly different tensile behaviours. The stress that can be sustained by Kirigami sheets is more than one order of magnitude smaller. However, the fracture strain is increased by more than a factor of 2. It can also be seen that four distinct stages of deformation occur in the Kirigami sheets prior to failure, as separated by the dashed lines in Fig. 2(a). Taking armchair Kirigami as an example, during the first stage the stress increases with rising strain at very low rate and does not exceed 1.0 GPa, while the critical strain reaches above 50%, unlike the deformation process of pristine h-BN nanosheets. By linear fitting the stress-strain curve of this stage, we can obtain a value of the Young's modulus E_1 of approximately 0.34 GPa. During this stage the Kirigami structure elongates along the loading direction without significantly stretching the B-N bonds, but mainly by lateral flapping of the cut sections and generating large out-of-plane rotations of the sides of the sheets, which involve

structural changes that require relatively little energy. The negligible stretch of the BN bonds, which is typical of elastic deformations since bond-stretching incurs a large energetic penalty, is confirmed by the predominance regular hexagonal B-N rings in the stretched sheet lattice, as shown in Fig. 2(b) a1, with little change in the bond lengths. This deformation mechanism is similar to that observed in graphene Kirigami, as in Ref [30]. It is the lateral flapping and rotation mechanism that generates the high ductility of the h-BN Kirigami sheets.

During Stage II, when the strain exceeds approximately 55% the stress-dependent strain increases at much higher rate than in Stage I (Fig. 2(a)), consistent with the main deformation mechanism now being purely elastic bond stretching rather than cut sections flipping and rotating. This change in deformation mechanism is confirmed from by inspecting the structure in Fig. 2(b); there is no further tendency of the cut sections to flap or rotate, while the regular hexagonal B-N rings distort because of stretching loading, and the cross-section of the sheet decreases significantly, as shown in Fig. 2(b) a2. The tangent modulus E_2 of this stage is about 18.95 GPa for the configuration considered (armchair). It should be noted that the total tensile strain after the first two stages reaches ~ 88%, a value much greater than the fracture strain of pristine h-BN nanosheets (about 30%). In Stage III bond breaking then takes place at higher strains, while the maximum stress varies between 6 GPa – 8 GPa, showing a pseudo ductile behaviour followed by the failure of the sheets (Fig. 2(a)). From Fig.2(b) it can be observed that at this stage local bond breaking near the edges of the cuts occurs, which is due to the high stress concentrations (as evident from the atom

stress distribution in Fig. 3). The largest stresses are concentrated near the edges of the each Kirigami geometric unit, as also previously observed in graphene Kirigami [30].

Finally, as shown in Fig.2 (b) a4, fracture occurs during Stage IV, after the tensile strain reaches 95%. For zigzag h-BN Kirigami, similar deformation phenomena were also observed.

Fig. 3 Stress distribution of armchair h-BN Kirigami prior to the failure corresponding to the snapshot in Fig. 2(b) a3. The data are scaled to lie between 0 and 1. This figure was generated using AtomEye [68].

3.2 Influence of the geometry parameters on the mechanical behaviour

The ductility and strength of the Kirigami h-BN sheets strongly depend upon the topology of the cut patterns, and therefore upon the dimensionless geometry parameters described above. To clearly understand the meaning of the variation of these parameters, different h-BN Kirigami configurations for the varying geometric parameters α, β and γ are shown in Fig. 4. Smaller values of the parameter α lead to a lower porosity of the Kirigami sheets, while larger values tend to produce configurations with larger voids and larger cuts heights. Large β leads to a lower density of the cuts (Fig. 4(b)).

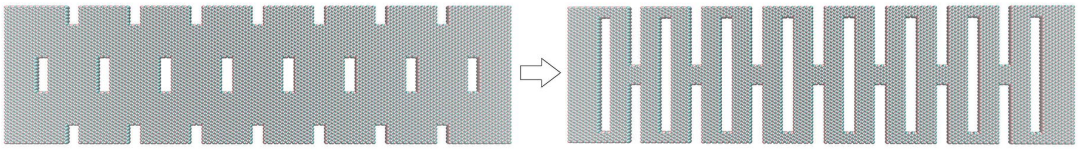

(a) increasing α with constant β and γ

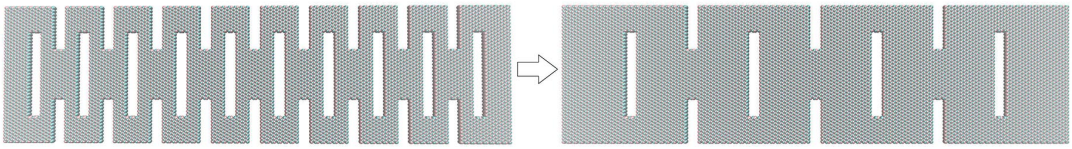

(b) increasing β with constant α and γ

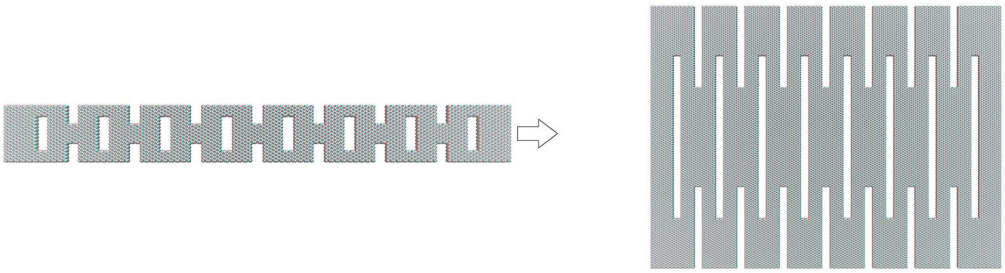

(c) decreasing γ with constant α and β

Fig. 4 Schematic Kirigami configurations for the varying geometric parameters α, β and γ

We have investigated the effects of these parameters on the global mechanical properties and deformation mechanisms of the Kirigami sheets. Figs 5 shows the complete stress-strain curves for armchair Kirigami sheets with different α but keeping constant β (0.0375) and γ (3.551). The stress-strain response of the Kirigami sheets is strongly affected by the cut height *w*. With increasing α, the ultimate strength firstly decreases significantly and then tends to be almost constant. When α is small (less than 0, as shown later) there is no evident initial low stiffness regime in the stress-strain curves (Stage I, as illustrated in Fig. 2(a)), and the fracture strains remain constant at ~ 20%, even slightly lower than the one of the pristine armchair h-BN sheets (23.6%). However, when α is increased there is an evident initial low rate

deformation stage in the corresponding stress-strain curves (Stage I). In this case the ultimate strength remains nearly constant at about 8GPa, while the fracture strain increases substantially with rising α. Thus, to enhance the ductility of the h-BN Kirigami, a large value of α should be adopted.

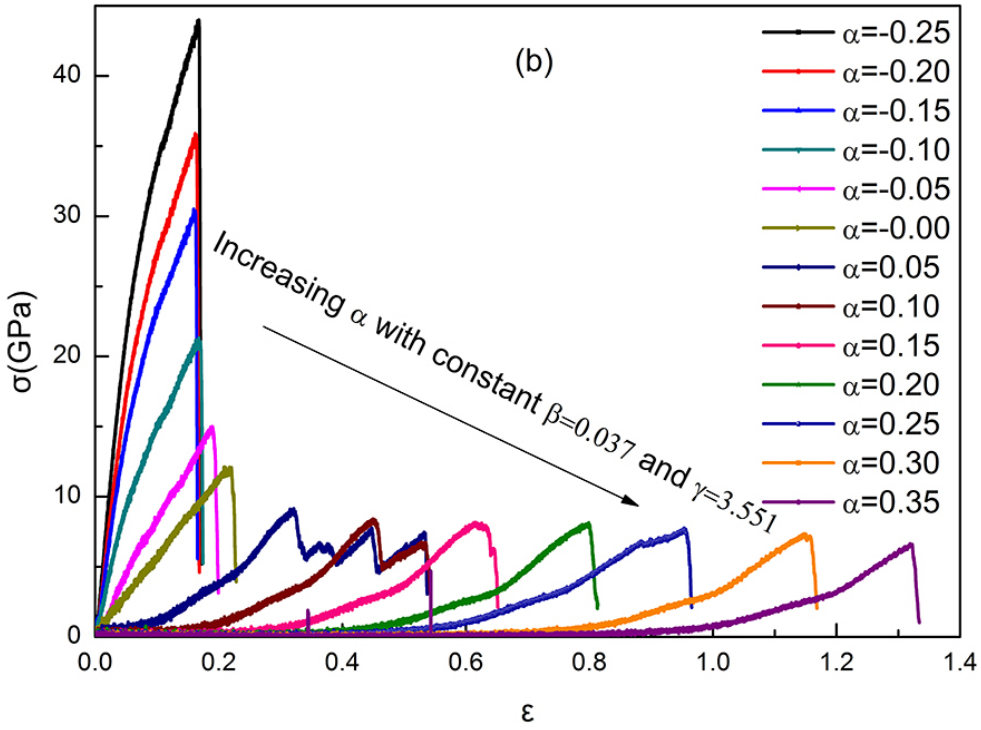

Fig. 5 Stress-strain curves for armchair Kirigami sheets keeping constant β= 0.0375, γ=3.551 and varying α (-0.25 < α < 0.35)

Fig. 6 shows the effect of α on the stress-strain relationship and ultimate strength and fracture strain of h-BN Kirigami for constant β and γ. In these and all subsequent figures, the stresses and strains are normalized by those for pristine h-BN nanoribbons of the same size so that the effect of the Kirigami parameters can be directly quantified. From Fig. 6(a) we see that the stress-strain relationships for zigzag Kirigami with different α show the same trend as armchair Kirigami (Fig. 5). The

ultimate strength and strain is plotted as a function of α in Figs. 6(b) and (c), respectively. It is clear that the ultimate stress of the Kirigami varies inversely with the cut width ratio, with the higher stresses corresponding to negative α parameters, and there is also a very low sensitivity of the stress to increasing positive α values for both armchair and zigzag configurations. In contrast, when $\alpha > 0$, the Kirigami becomes significantly more ductile, as shown in Fig. 6(c), where the fracture strains for armchair and zigzag Kirigami are approximately 2.5 and 5 times larger, respectively, than that of the pristine nanoribbon. However, when $\alpha < 0$, the fracture strains tend to be insensitive to the value of α for both armchair and zigzag Kirigami and we also note that in this regime the strains, especially for the zigzag form, are even lower than that of the pristine h-BN nanoribbon.

The overall deformation mechanism at different α values can be rationalised as follows. As illustrated in Fig. 1 and Fig. 4, $\alpha = 0$ corresponds to the configuration in which the edge and the interior cuts just begin to overlap. When $\alpha < 0$, the edge and the interior cuts do not overlap and out-of-plane deformation tends to be severely constrained, or does not even occur at lower α. In this case, the cuts can be viewed as atomic line defects which may decrease the strength and strain substantially. The smaller is α, the higher is the strength, which approaches that of the cut-free nanoribbon. In contrast, when $\alpha > 0$ the flipping and rotation mechanism of Fig.2 (b) a1 takes place, which contributes largely to large stretching and compliance of the Kirigami configuration. Increasing overlap of edge and interior cuts leads to increasing ductility of the h-BN Kirigami nanoribbon.

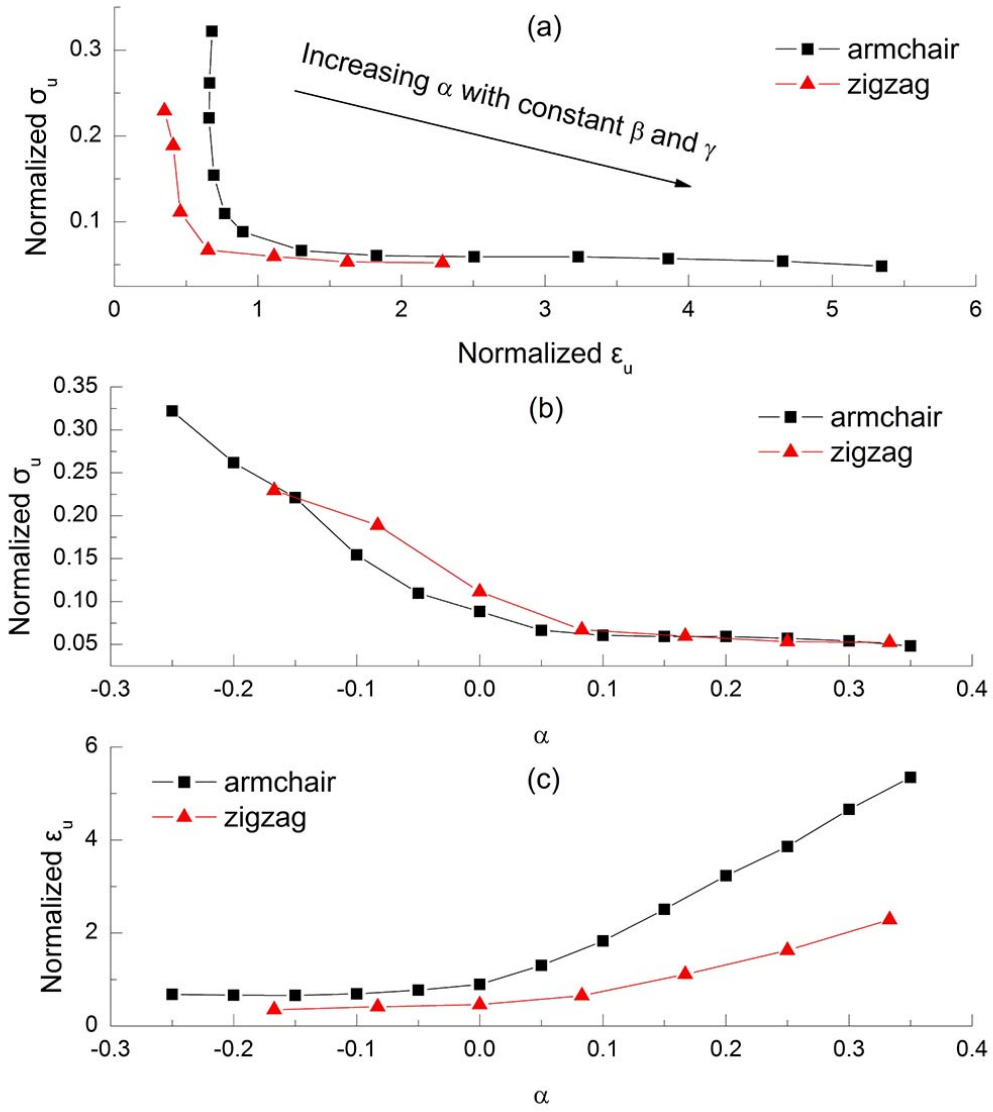

Fig.6 Effects of α (-0.25 < α < 0.35) on the (a) stress-strain relationship (b) ultimate strength and (c) fracture strain of h-BN Kirigami for constant β and γ. For armchair β =0.037, γ=3.551, and for zigzag β =0.056, γ=3.416. Data are normalized by pristine h-BN nanoribbon results with the same size.

The effects of β on the stress-strain relationship, ultimate strength and fracture strain of the h-BN Kirigami nanostructure for constant α and γ are shown in Fig. 7. In this case the different Kirigami configurations are produced by varying the cut unit cell width *d* from 2.5 nm to 8.7 nm , while keeping all other geometry parameters constant.

This parameter has a large effect on the mechanical properties of both armchair and zigzag h-BN Kirigami. As illustrated in Fig. 4, large β values lead to decreased amounts of cut unit cell and lower density of the cuts, which results in a reduction in operation of the out-of-plane deformation mechanism we have discussed. Thus, as shown in Figs. 7 (b) and (c), increasing β leads to a decrease in fracture strain and an increase in ultimate strength. Note in particular that when, approximately, $\beta > 0.06$ (zigzag) or >0.08 (armchair), the fracture strain of both Kirigami forms is even lower than that of the pristine h-BN nanoribbon. This is due to the presence of the cut patterns, which can be viewed as line atomic defects, which once again can decrease the ultimate stress and fracture strain of the h-BN nanoribbon.

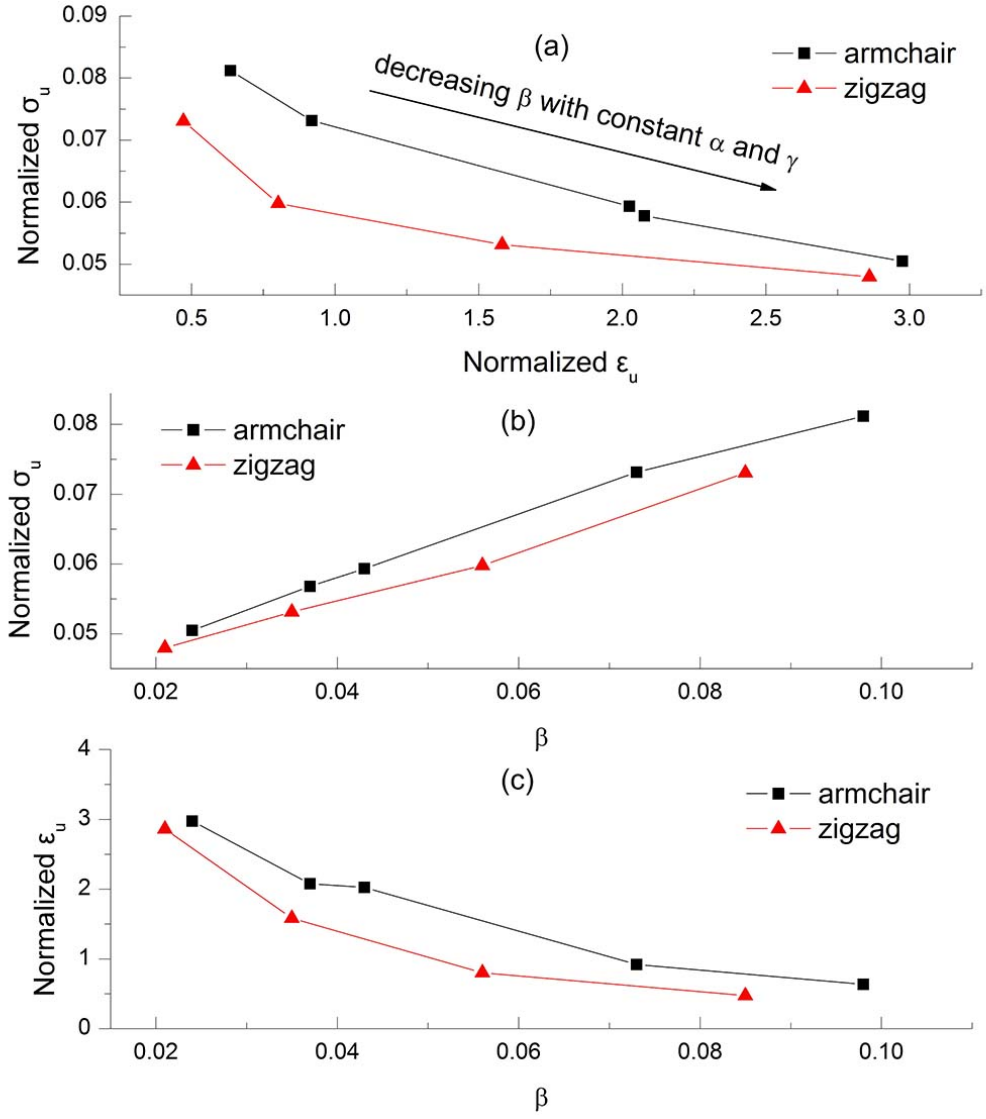

Fig.7 Effects of β (0.021 < β < 0.099) on the (a) stress-strain relationship (b) ultimate strength and (c) fracture strain of h-BN Kirigami for constant α and γ. α =0.125, and γ=3.551, 3.416 for armchair and zigzag, respectively. Data are normalized by pristine h-BN nanoribbon results with the same size.

Besides varying α and β we have also examined the influence of the length-to-width ratio γ on the mechanical behavior of h-BN Kirigami (Fig. 8). This is achieved by changing the ratio of the length and width of the Kirigami nanoribbons to keep the parameters α and β constant. Here we changed b and w, keeping L_0, c and d constant. Figs. 8(b) and (c) show that for both armchair and zigzag configurations decreasing γ results in an almost linear increase in ultimate strength, and a monotonic decrease in fracture strain. For $\gamma > 4$–~6, the ultimate strength increases with γ, the variation in fracture strain is much less.

The behaviour of the h-BN Kirigami nanoribbons tends to mirror that of graphene-based Kirigami systems [30]. Normalised fracture strains in graphene Kirigami tend to be higher for armchair configurations with larger values of α, as in our simulations. Zigzag graphene Kirigami with α=0.1 and β=0.057 have a normalised fracture strain close to 2.5 [30]. However the failure value for analogous zigzag h-BN Kirigami with a similar configuration is less than unity, indicating that larger values of α are needed for a high fracture strain. Armchair h-BN configurations have larger fracture strains (~2) when β is small and high normalised fracture strains when α is large ($\varepsilon_U > 5$). For fracture failure, there are notable differences between armchair and zigzag graphene and h-BN Kirigami; for α~0.05 and β~0.06 the armchair graphene topology has a normalised fracture stress of 0.116 while the zigzag value is 0.087; for the h-BN analogue, the armchair value is 0.066 while the zigzag is 0.085. Comparing our results with previous studies, we can observe that h-BN and graphene Kirigami possess different mechanical parameters, which are typical of the

their core materials properties. The Kirigami structures have however similar strain-dependent behaviours, which are essentially caused by their intrinsic geometry. The results shown in this work indicate the presence of the same mechanisms to enhance the ductility, i.e. the lateral flapping and out-of-plane rotation of the Kirigami sheets.

Overall in our simulations the ductility of the h-BN Kirigami was increased by increasing the overlapping cut (increasing parameter α), increasing the amount of geometric cut unit (decreasing parameter β), and increasing length-to-width ratio (increasing parameter γ). It should also be pointed out that although incorporating Kirigami patterns can significantly enhance the ductility of h-BN, the elastic properties or Young's Modulus and the strength of Kirigami structures are significantly decreased compared to h-BN nanoribbons (up to 60~90% - see Figs. 6-8). During the tensile loading the Kirigami-patterned sheets exhibit out-of-plane deformations, and failure begins when the ends of the cuts tear and crease through because of the high stress concentrations in these regions. To further the latter, one could employ a technique widely used in fracture mechanics, i.e., the blunting of the crack tip using a stress distributing geometry, such as circles or rectangles with half circles. These circular features can effectively delay the onset of tearing and crack propagation, and thus can improve the strain to failure of the Kirigami structures compared to the rectangular cut patterns studied in this work, although the magnitude of the strength to failure may also decrease. Another approach may consist in the adoption of bridging materials, or distribution of polymeric molecules that may ease

the intensity of the stress concentrations.

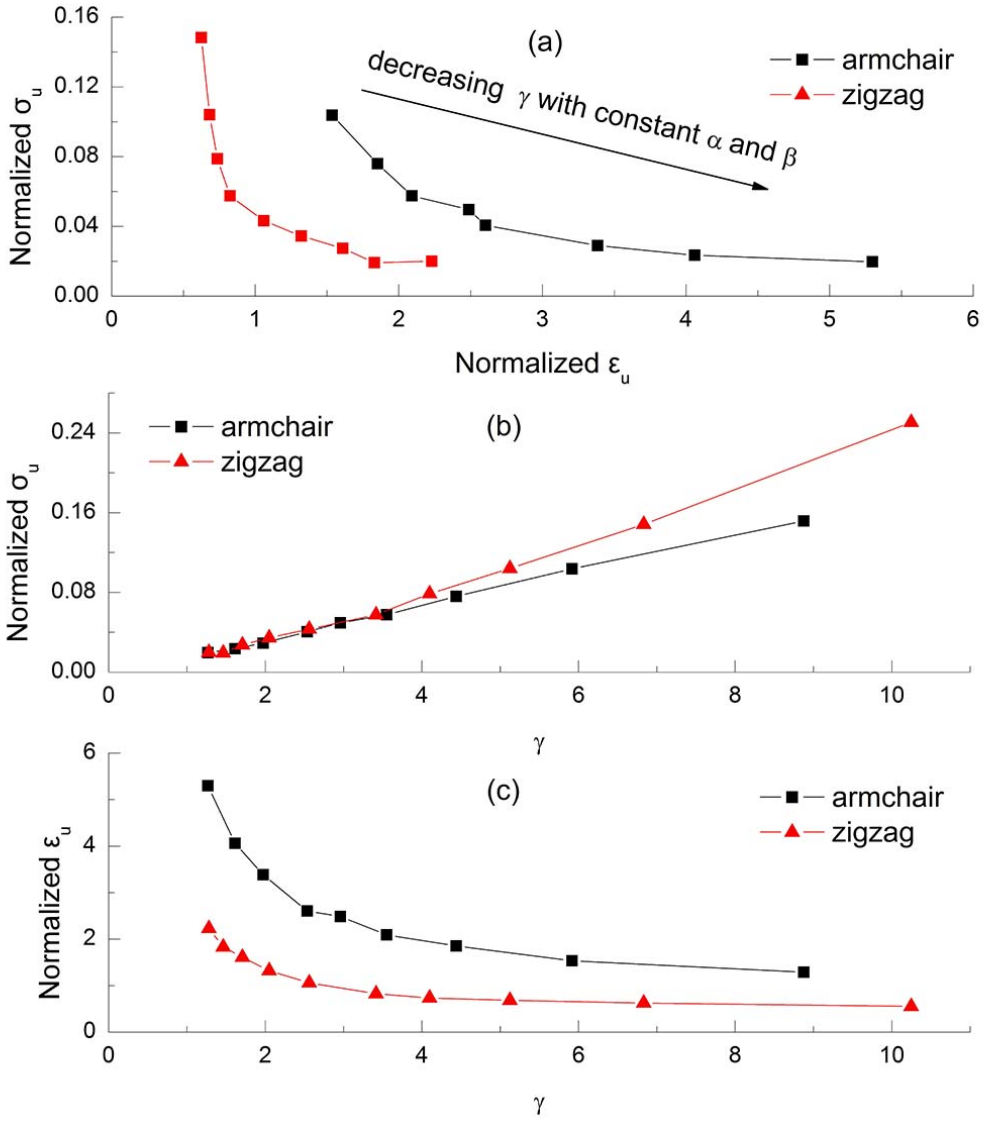

Fig.8 Effects of γ (1.27 < γ < 10.25) on the (a) stress-strain relationship (b) ultimate strength and (c) fracture strain of h-BN Kirigami for constant α and β. α =0.125, and β=0.037, 0.056 for armchair and zigzag, respectively. The data are normalized by pristine h-BN nanoribbon results with the same size.

4. Conclusions

In this study we have performed classical molecular dynamics simulations to

investigate the mechanical behaviour of hexagonal boron nitride Kirigami structures. The effects on the mechanical behavior caused by the topology of the cut patterns and the scale aspects (defined by three key geometry parameters) have also been studied and analysed systematically. The results indicate that Kirigami patterning is an effective way to enhance dramatically the bilinearity and stretching capability of h-BN nanosheets. The resulting enhancements in fracture strains can be as much as a fivefold increase over the values for pristine h-BN nanoribbons. These results suggest that the Kirigami architectural approach may constitute a suitable technique to design super-ductile two-dimensional nanomaterials and may open up a wide range of novel technological solutions for stretchable electronics and optoelectronic devices, in particular when bio-compatibility with the environment is a constraint for the design of these nanosensors.

Acknowledgments

We greatly appreciate the financial support of the Jiangsu Overseas Research & Training Program for University Prominent Young & Middle-aged Teachers and Presidents and the Natural Science Foundation of Jiangsu Province of China (No. BK2011490). The Authors would also like to thank the Reviewers for their constructive comments.

References

[1] K.S. Novoselov, A.K. Geim, S.V. Morozov, D. Jiang, Y. Zhang, S.V. Dubonos, I.V. Grigorieva, A.A. Firsov, Electric field effect in atomically thin carbon films, Science, 306 (2004) 666-669.

[2] K.S. Novoselov, D. Jiang, F. Schedin, T.J. Booth, V.V. Khotkevich, S.V. Morozov, A.K. Geim, Two-dimensional atomic crystals, Proc. Natl. Acad. Sci. U. S. A., 102 (2005) 10451-10453.

[3] Y. Wang, C.H. Zhou, W.C. Wang, Y.P. Zhao, Preparation of Two Dimensional Atomic Crystals BN, WS2, and MoS2 by Supercritical CO2 Assisted with Ultrasound, Ind. Eng. Chem. Res., 52 (2013)

4379-4382.
[4] H.S.S.R. Matte, A. Gomathi, A.K. Manna, D.J. Late, R. Datta, S.K. Pati, C.N.R. Rao, MoS2 and WS2 Analogues of Graphene, Angewandte Chemie-International Edition, 49 (2010) 4059-4062.
[5] A. Nag, K. Raidongia, K.P.S.S. Hembram, R. Datta, U.V. Waghmare, C.N.R. Rao, Graphene Analogues of BN: Novel Synthesis and Properties, Acs Nano, 4 (2010) 1539-1544.
[6] H.B. Zeng, C.Y. Zhi, Z.H. Zhang, X.L. Wei, X.B. Wang, W.L. Guo, Y. Bando, D. Golberg, "White Graphenes": Boron Nitride Nanoribbons via Boron Nitride Nanotube Unwrapping, Nano Lett., 10 (2010) 5049-5055.
[7] W.S. Hwang, M. Remskar, R.S. Yan, V. Protasenko, K. Tahy, S.D. Chae, P. Zhao, A. Konar, H.L. Xing, A. Seabaugh, D. Jena, Transistors with chemically synthesized layered semiconductor WS2 exhibiting 10(5) room temperature modulation and ambipolar behavior, Appl. Phys. Lett., 101 (2012) 013107.
[8] X. Blase, A. Rubio, S.G. Louie, M.L. Cohen, Stability and Band-Gap Constancy of Boron-Nitride Nanotubes, Europhys. Lett., 28 (1994) 335-340.
[9] Z.H. Zhang, W.L. Guo, Y.T. Dai, Stability and electronic properties of small boron nitride nanotubes, J. Appl. Phys., 105 (2009) 084312.
[10] Y. Chen, J. Zou, S.J. Campbell, G. Le Caer, Boron nitride nanotubes: Pronounced resistance to oxidation, Appl. Phys. Lett., 84 (2004) 2430-2432.
[11] N.G. Chopra, A. Zettl, Measurement of the elastic modulus of a multi-wall boron nitride nanotube, Solid State Commun., 105 (1998) 297-300.
[12] T. Dumitrica, H.F. Bettinger, G.E. Scuseria, B.I. Yakobson, Thermodynamics of yield in boron nitride nanotubes, Physical Review B, 68 (2003) 085412.
[13] D. Golberg, Y. Bando, Y. Huang, T. Terao, M. Mitome, C.C. Tang, C.Y. Zhi, Boron Nitride Nanotubes and Nanosheets, Acs Nano, 4 (2010) 2979-2993.
[14] R. Arenal, M.S. Wang, Z. Xu, A. Loiseau, D. Golberg, Young modulus, mechanical and electrical properties of isolated individual and bundled single-walled boron nitride nanotubes, Nanotechnology, 22 (2011) 265704.
[15] R. Kumar, A. Parashar, Atomistic modeling of BN nanofillers for mechanical and thermal properties: a review, Nanoscale, 8 (2016) 22-49.
[16] G. Ciofani, S. Danti, G.G. Genchi, B. Mazzolai, V. Mattoli, Boron Nitride Nanotubes: Biocompatibility and Potential Spill-Over in Nanomedicine, Small, 9 (2013) 1672-1685.
[17] C.R. Dean, A.F. Young, I. Meric, C. Lee, L. Wang, S. Sorgenfrei, K. Watanabe, T. Taniguchi, P. Kim, K.L. Shepard, J. Hone, Boron nitride substrates for high-quality graphene electronics, Nature Nanotechnology, 5 (2010) 722-726.
[18] C.Y. Zhi, Y. Bando, C.C. Tang, H. Kuwahara, D. Golberg, Large-Scale Fabrication of Boron Nitride Nanosheets and Their Utilization in Polymeric Composites with Improved Thermal and Mechanical Properties, Adv. Mater., 21 (2009) 2889-2893.
[19] Y.W. Gao, A.J. Gu, Y.C. Jiao, Y.L. Yang, G.Z. Liang, J.T. Hu, W. Yao, L. Yuan, High-performance hexagonal boron nitride/bismaleimide composites with high thermal conductivity, low coefficient of thermal expansion, and low dielectric loss, Polym. Adv. Technol., 23 (2012) 919-928.
[20] F.S. Lu, F. Wang, L. Cao, C.Y. Kong, X.C. Huang, Hexagonal Boron Nitride Nanomaterials: Advances Towards Bioapplications, Nanoscience and Nanotechnology Letters, 4 (2012) 949-961.
[21] A. Pakdel, C.Y. Zhi, Y. Bando, D. Golberg, Low-dimensional boron nitride nanomaterials, Mater.

Today, 15 (2012) 256-265.
[22] C. Li, Y. Bando, C.Y. Zhi, Y. Huang, D. Golberg, Thickness-dependent bending modulus of hexagonal boron nitride nanosheets, Nanotechnology, 20 (2009) 385707.
[23] T.W. Han, Y. Luo, C.Y. Wang, Effects of temperature and strain rate on the mechanical properties of hexagonal boron nitride nanosheets, J. Phys. D: Appl. Phys., 47 (2014) 025303.
[24] C. Si, Z. Sun, F. Liu, Strain engineering of graphene: a review, Nanoscale, 8 (2016) 3207-3217.
[25] K. Saito, F. Agnese, F. Scarpa, A Cellular Kirigami Morphing Wingbox Concept, J. Intell. Mater. Syst. Struct., 22 (2011) 935-944.
[26] Y. Hou, R. Neville, F. Scarpa, C. Remillat, B. Gu, M. Ruzzene, Graded conventional-auxetic Kirigami sandwich structures: Flatwise compression and edgewise loading, Composites Part B-Engineering, 59 (2014) 33-42.
[27] T. Nojima, K. Saito, Development of newly designed ultra-light core structures, Jsme International Journal Series a: Solid Mechanics and Material Engineering, 49 (2006) 38-42.
[28] M.K. Blees, A.W. Barnard, P.A. Rose, S.P. Roberts, K.L. McGill, P.Y. Huang, A.R. Ruyack, J.W. Kevek, B. Kobrin, D.A. Muller, P.L. McEuen, Graphene kirigami, Nature, 524 (2015) 204-207.
[29] P.Z. Hanakata, Z.A. Qi, D.K. Campbell, H.S. Park, Highly stretchable MoS2 kirigami, Nanoscale, 8 (2016) 458-463.
[30] Z.N. Qi, D.K. Campbell, H.S. Park, Atomistic simulations of tension-induced large deformation and stretchability in graphene kirigami, Physical Review B, 90 (2014) 245437.
[31] S. Plimpton, Fast Parallel Algorithms for Short-Range Molecular-Dynamics, Journal of Computational Physics, 117 (1995) 1-19.
[32] J. Tersoff, New empirical approach for the structure and energy of covalent systems, Physical Review B, 37 (1988) 6991-7000.
[33] J. Tersoff, Empirical Interatomic Potential for Carbon, with Applications to Amorphous Carbon, Phys. Rev. Lett., 61 (1988) 2879-2882.
[34] J. Tersoff, Modeling solid-state chemistry: Interatomic potentials for multicomponent systems, Physical Review B, 39 (1989) 5566-5568.
[35] S. Ebrahimi-Nejad, A. Shokuhfar, Compressive buckling of open-ended boron nitride nanotubes in hydrogen storage applications, Physica E, 50 (2013) 29-36.
[36] A. Ali Shokuhfar, S. Ebrahimi-Nejad, Effects of structural defects on the compressive buckling of boron nitride nanotubes, Physica E, 48 (2013) 53-60.
[37] J. Song, J. Wu, Y. Huang, K.C. Hwang, Continuum modeling of boron nitride nanotubes, Nanotechnology, 19 (2008) 445705.
[38] Q.L. Xiong, Z.H. Li, X.G. Tian, The defect-induced fracture behaviors of hexagonal boron-nitride monolayer nanosheets under uniaxial tension, J. Phys. D: Appl. Phys., 48 (2015) 375502.
[39] W. Sekkal, B. Bouhafs, H. Aourag, M. Certier, Molecular-dynamics simulation of structural and thermodynamic properties of boron nitride, Journal of Physics-Condensed Matter, 10 (1998) 4975-4984.
[40] V. Verma, V.K. Jindal, K. Dharamvir, Elastic moduli of a boron nitride nanotube, Nanotechnology, 18 (2007) 435711.
[41] K. Matsunaga, Y. Iwamoto, Molecular dynamics study of atomic structure and diffusion behavior in amorphous silicon nitride containing boron, J. Am. Ceram. Soc., 84 (2001) 2213-2219.
[42] K. Albe, W. Moller, Modelling of boron nitride: Atomic scale simulations on thin film growth, Computational Materials Science, 10 (1998) 111-115.

[43] K. Albe, W. Moller, K.H. Heinig, Computer simulation and boron nitride, Radiat Eff. Defects Solids, 141 (1997) 85-97.
[44] A. Kinaci, J.B. Haskins, C. Sevik, T. Cagin, Thermal conductivity of BN-C nanostructures, Physical Review B, 86 (2012) 115410.
[45] C. Sevik, A. Kinaci, J.B. Haskins, T. Cagin, Characterization of thermal transport in low-dimensional boron nitride nanostructures, Physical Review B, 84 (2011) 085409.
[46] K. Matsunaga, C. Fisher, H. Matsubara, Tersoff potential parameters for simulating cubic boron carbonitrides, Jpn. J. Appl. Phys., Part 2, 39 (2000) 48-51.
[47] H. Shen, Thermal-conductivity and tensile-properties of BN, SiC and Ge nanotubes, Computational Materials Science, 47 (2009) 220-224.
[48] G.J. Slotman, A. Fasolino, Structure, stability and defects of single layer hexagonal BN in comparison to graphene, Journal of Physics-Condensed Matter, 25 (2013) 045009.
[49] D.M. Tang, C.L. Ren, X.L. Wei, M.S. Wang, C. Liu, Y. Bando, D. Golberg, Mechanical Properties of Bamboo-like Boron Nitride Nanotubes by In Situ TEM and MD Simulations: Strengthening Effect of Interlocked Joint Interfaces, Acs Nano, 5 (2011) 7362-7368.
[50] M.Q. Le, Atomistic Study on the Tensile Properties of Hexagonal AlN, BN, GaN, InN and SiC Sheets, Journal of Computational and Theoretical Nanoscience, 11 (2014) 1458-1464.
[51] Y.B. Zhao, X.H. Peng, T. Fu, C. Huang, C. Feng, D.Q. Yin, Z.C. Wang, Molecular dynamics simulation of nano-indentation of (111) cubic boron nitride with optimized Tersoff potential, Appl. Surf. Sci., 382 (2016) 309-315.
[52] Q.L. Xiong, Z.H. Li, X.G. Tian, The defect-induced fracture behaviors of hexagonal boron-nitride monolayer nanosheets under uniaxial tension, J Phys D Appl Phys, 48 (2015) 375502.
[53] W.C. Swope, H.C. Andersen, P.H. Berens, K.R. Wilson, A Computer-Simulation Method for the Calculation of Equilibrium-Constants for the Formation of Physical Clusters of Molecules - Application to Small Water Clusters, J. Chem. Phys., 76 (1982) 637-649.
[54] S. Nose, A Molecular-Dynamics Method for Simulations in the Canonical Ensemble, Mol. Phys., 52 (1984) 255-268.
[55] W.G. Hoover, Canonical Dynamics: Equilibrium Phase-Space Distributions, Physical Review A, 31 (1985) 1695-1697.
[56] A.P. Thompson, S.J. Plimpton, W. Mattson, General formulation of pressure and stress tensor for arbitrary many-body interaction potentials under periodic boundary conditions, J. Chem. Phys., 131 (2009) 154107.
[57] A. Bosak, J. Serrano, M. Krisch, K. Watanabe, T. Taniguchi, H. Kanda, Elasticity of hexagonal boron nitride: Inelastic x-ray scattering measurements, Physical Review B, 73 (2006) 041402.
[58] N. Ohba, K. Miwa, N. Nagasako, A. Fukumoto, First-principles study on structural, dielectric, and dynamical properties for three BN polytypes, Physical Review B, 63 (2001) 115207.
[59] M. Mirnezhad, R. Ansari, H. Rouhi, Mechanical properties of multilayer boron nitride with different stacking orders, Superlattices Microstruct., 53 (2013) 223-231.
[60] B. Mortazavi, Y. Remond, Investigation of tensile response and thermal conductivity of boron-nitride nanosheets using molecular dynamics simulations, Physica E, 44 (2012) 1846-1852.
[61] S.J. Zhao, J.M. Xue, Mechanical properties of hybrid graphene and hexagonal boron nitride sheets as revealed by molecular dynamic simulations, J. Phys. D: Appl. Phys., 46 (2013) 135303-135311.
[62] L. Boldrin, F. Scarpa, R. Chowdhury, S. Adhikari, Effective mechanical properties of hexagonal boron nitride nanosheets, Nanotechnology, 22 (2011) 505702.

[63] E.S. Oh, Elastic properties of boron-nitride nanotubes through the continuum lattice approach, Mater. Lett., 64 (2010) 859-862.
[64] X.L. Wei, M.S. Wang, Y. Bando, D. Golberg, Tensile Tests on Individual Multi-Walled Boron Nitride Nanotubes, Adv. Mater., 22 (2010) 4895–4899.
[65] D.V. Fakhrabad, N. Shahtahmassebi, First-principles calculations of the Young's modulus of double wall boron-nitride nanotubes, Mater. Chem. Phys., 138 (2013) 963-966.
[66] L.Y. Zhang, Y.J. Peng, Q.H. Jin, Y.F. Wang, B.H. Li, D.T. Ding, Elastic properties of single-wall nanotubes, Acta Phys Sin-ch Ed, 55 (2006) 4193-4196.
[67] W. Humphrey, A. Dalke, K. Schulten, VMD: Visual molecular dynamics, J. Mol. Graph. Model., 14 (1996) 33-38.
[68] J. Li, AtomEye: an efficient atomistic configuration viewer, Modell. Simul. Mater. Sci. Eng., 11 (2003) 173-177.

Figure captions

Fig.1 Schematic simulation model of the h-BN Kirigami tested, with the key geometric parameters labelled.

Fig.2 (a) Stress-strain curves of the representative armchair and zigzag h-BN Kirigami. Four distinct stages of deformation occur in the Kirigami sheets prior to failure, as shown in Fig. 2(a) by the dashed lines for armchair Kirigami. Stress-strain curves of pristine armchair and zigzag h-BN are also shown in the inset for comparison. (b) Snapshots of the top view of the atom configuration of the armchair h-BN Kirigami. The tensile strains corresponding to the different stages are 30%, 78%, 91%, 96.3%, respectively. The snapshots were generated by Visual Molecular Dynamics (VMD).

Fig. 3 Stress distribution of armchair h-BN Kirigami prior to the failure corresponding to the snapshot in Fig. 2(b) a3, where the data were scaled between 0 and 1. This figure was generated by AtomEye.

Fig. 4 Schematic Kirigami configurations for varying geometric parameters α, β and γ

Fig. 5 Stress-strain curves for armchair Kirigami sheets keeping constant β= 0.0375, γ=3.551 and varying α ($-0.25 < \alpha < 0.35$)

Fig.6 Effects of α ($-0.25 < \alpha < 0.35$) on the (a) stress-strain relationship (b) ultimate strength and (c) fracture strain of h-BN Kirigami for constant β and γ. For armchair β =0.037, γ=3.551, and for zigzag β =0.056, γ=3.416. Data are normalized by pristine h-BN nanoribbon results with the same size.

Fig.7 Effects of β ($0.021 < \beta < 0.099$) on the (a) stress-strain relationship (b) ultimate

strength and (c) fracture strain of h-BN Kirigami for constant α and γ. α =0.125, and γ=3.551, 3.416 for armchair and zigzag, respectively. Data are normalized by pristine h-BN nanoribbon results with the same size.

Fig.8 Effects of γ ($1.27 < \gamma < 10.25$) on the (a) stress-strain relationship (b) ultimate strength and (c) fracture strain of h-BN Kirigami for constant α and β. α =0.125, and β=0.037, 0.056 for armchair and zigzag, respectively. The data are normalized by pristine h-BN nanoribbon results with the same size.